

Designing of new tetrahydro- β -carboline-based ABCG2 inhibitors using 3D-QSAR, molecular docking, and DFT tools

Shahnawaz Ahmad, Dinesh Gupta, Tanzeel Ahmed & Asimul Islam

To cite this article: Shahnawaz Ahmad, Dinesh Gupta, Tanzeel Ahmed & Asimul Islam (2023): Designing of new tetrahydro- β -carboline-based ABCG2 inhibitors using 3D-QSAR, molecular docking, and DFT tools, Journal of Biomolecular Structure and Dynamics, DOI: 10.1080/07391102.2023.2176361

To link to this article: <https://doi.org/10.1080/07391102.2023.2176361>

 View supplementary material 

 Published online: 08 Feb 2023.

 Submit your article to this journal 

 View related articles 

 View Crossmark data 



Designing of new tetrahydro- β -carboline-based ABCG2 inhibitors using 3D-QSAR, molecular docking, and DFT tools

Shahnawaz Ahmad^{a,b} , Dinesh Gupta^c, Tanzeel Ahmed^a and Asimul Islam^b

^aSchool of Biotechnology, College of Engineering and Technology, IFTM University, Moradabad, Uttar Pradesh, India; ^bCentre for Interdisciplinary Research in Basic Sciences, Jamia Millia Islamia, New Delhi, India; ^cTranslational Bioinformatics Group, International Centre for Genetic Engineering and Biotechnology (ICGEB), Aruna Asaf Ali Marg, New Delhi, India

Communicated by Ramaswamy H. Sarma

ABSTRACT

Human ATP-binding cassette superfamily G member 2 (ABCG2) protein is a member of the ABC transporter family, which is responsible for multidrug resistance (MDR) in cancerous cells. MDR reduces the effectiveness of chemotherapy in breast cancer, which is one of the leading causes of death in women globally. MDR in cancer cells is one of the immediate signs of progression of resistance; thus, various anticancer drugs can be designed. To reduce MDR, we utilized the tetrahydro- β -carboline (TH β C) compound library. We accomplished a three-dimensional quantitative structure-activity relationship (3D-QSAR), scaffold hopping to design a new library of compounds of TH β C, and further molecular docking, induced-fit docking (IFD), molecular mechanics energies combined with generalized born and surface area continuum solvation (MM-GBSA), drug-like features, ADMET properties, and density functional theory (DFT) studies were performed. From these studies, the best 3D-QSAR model ($r^2 = 0.99$, $q^2 = 0.92$) was found, and the necessity of electrostatic, steric, and hydrophobic field effects were determined that could modulate bioactivity. Moreover, based on electrostatic, steric, and hydrophobic field notations, new TH β C derivatives (3409) were designed. These findings might provide new insight for researchers to perform *in vitro* and *in vivo* studies for better antagonists against MDR in treating breast cancer.

Abbreviations: ABCG2: ATP-binding cassette superfamily G member 2; ADMET: Absorption, distribution, metabolism, excretion and toxicity; BC: breast cancer; DFT: density functional theory; 3D-QSAR: three-dimensional quantitative structure-activity relationship; HOMO: highest occupied molecular orbital; IFD: induced-fit docking; LOOCV: leave one out cross-validation; LUMO: lowest unoccupied molecular orbital; MDR: multidrug resistance; MM-GBSA: molecular mechanics energies combined with generalized born and surface area continuum solvation; ND-TH β C: newly designed tetrahydro- β -carboline; q^2 : cross-validation regression coefficient; r^2 : correlation coefficient; XED: eXtended Electron Distribution

ARTICLE HISTORY

Received 19 December 2022
Accepted 30 January 2023

KEYWORDS

Breast cancer; ABCG2; 3D-QSAR; Scaffold hopping; Molecular docking; DFT; MM-GBSA; IFD; Activity Atlas model

1. Introduction

Cancer is one of the non-communicable disease in which cells divide by an uncontrollable pathway and can invade adjacent/other tissues that can affect any part of the body (Ahmad et al., 2022; Arnold et al., 2022). The risk factors of cancer include external environmental factors, genetic and epigenetic factors, dietary factors, high body mass index, lack of physical exercise, and excess use of tobacco and alcohol. Early age of first menstruation, older age, and family history can also cause cancers (Mohammad et al., 2018). It is considered one of the deadliest diseases globally, where the most common cancers are found in females, such as breast cancer (BC) (Ahmad et al., 2022). According to the WHO reports, BC became the most common cancer in 2021, constituting 12% of all the new annual cancer cases (Patel et al., 2021). In 2020, 2.3 million women were

diagnosed with BC resulting in 0.6 million deaths (Arnold et al., 2022). Among all cancer-causing protein families, ATP-binding cassette superfamily G member 2 (ABCG2) is one of the major factors responsible for causing multidrug resistance (MDR) in various cancer cells, including those of BC (Mohammad et al., 2018). ABCG2 is an ATP-dependent transporter belonging to the ATP binding cassette family located on the 4q22.1 position on chromosome 4 with a molecular mass of 72 kDa (Patel et al., 2021; Moinul et al., 2022; Taylor et al., 2017). It has been identified as a breast cancer resistance protein (BCRP), which physiologically functions in a self-defense mechanism in eliminating toxic xenobiotics through various barriers (Nakanishi & Ross, 2012). The protein is identified as one of the essential therapeutic biomarkers expressed in cancers which directly affects the efflux

CONTACT Asimul Islam  aislam@jmi.ac.in  Centre for Interdisciplinary Research in Basic Sciences, Jamia Millia Islamia, New Delhi, India; Tanzeel Ahmed  tanzeel_ahmad@iftmuniversity.ac.in  School of Biotechnology, College of Engineering and Technology, IFTM University, Lodhipur-Rajput, Delhi Road (NH-24), Moradabad, Uttar Pradesh 244102, India.

 Supplemental data for this article can be accessed online at <https://doi.org/10.1080/07391102.2023.2176361>.

mechanism and metabolic/signaling pathways, resulting in poor prognosis (Chun et al., 2017).

Tetrahydro- β -carboline (TH β C) is an alkaloid compound found in many natural products (NPs) and synthetic compounds with various pharmacological activities (Wang et al., 2021). TH β C, a member of the beta-carboline family, consists of a rigid indole ring and a flexible piperidine motif (Wang et al., 2021). The semi-rigid structure forming TH β C shows varying affinity against different receptors and could be used as both an H-bond acceptor and donor in drug design. Furthermore, the TH β C and its derivatives are widely used in the design of drugs against viruses, cancers, Alzheimer's, and several other disorders (Song et al., 2014; Xing et al., 2022; Liu et al., 2022). Recently, TH β C has gained interest as an ABCG2 inhibitor (Spindler et al., 2016). Owing to its promising biological activity, this work was carried out to design new TH β C as ABCG2 inhibitors and identify structural requirements to endow high activity. The reference molecule was extracted from a library of 30 TH β C compounds reported earlier (Spindler et al., 2016). 3D-QSAR was performed, and electrostatic, steric, and hydrophobic field effects were obtained that could modulate the bioactivity of the molecules. This is followed by an extensive scaffold hopping, molecular docking, molecular mechanics energies combined with generalized born and surface area continuum solvation (MM-GBSA), and density functional theory (DFT) calculations on a series of newly designed compounds.

Additionally, molecular docking of ABCG2 with 30 TH β C compounds were also performed. Based on the results, compound 27 was selected as a highly bioactive compound for further analysis. Scaffold hopping using compound 27 as an input to utilize on the inbuilt Spark-Cresset databases such as ChEMBL, ZINC database, VEHICLE (ring systems), and eMolecules and 3409 novel compounds were designed. Further, we used the Flare module of Cresset and Schrödinger to perform high throughput virtual screening, molecular docking, and induced-fit docking (IFD) of the newly formed compounds against the ABCG2 receptor to quantify the ligand binding potential. Top-scoring compounds were further subjected to drug likeliness, Lipinski's rule of five (RO5), and absorption, distribution, metabolism, excretion, and toxicity (ADMET) property analysis using the QikProp-Schrödinger. Furthermore, the molecules were examined for comparative MM-GBSA studies by Prime-Schrödinger to acquire the free binding energies (ΔG_{bind}). Finally, one mitoxantrone drug molecule as control, compound 27 from the earlier synthesized, and the top four compounds from the newly designed (ND) dataset were selected for DFT calculations. Eventually, we propose four ND-TH β C compounds, i.e. NDTH β C1 to NDTH β C4, as putative potential inhibitors of ABCG2, which might provide future insights into the experimental validations in the anti-cancer regimen.

2. Material and methods

2.1. Computational resources and data acquisition

The work was carried out on Tyrone workstation with 124 GB RAM; NVIDIA graphics card (GPU v100 32 GB); installed. The

workstation is installed with various bioinformatics software such as Schrödinger (v12.8.117), Cresset modules (Cresset Inc., Cambridgeshire, UK), and Spartan20 (Deppmeier et al., 2002; Amaro et al., 2018). The 3D structure of the ABCG2 protein and the co-crystallized drug mitoxantrone, used as a control, were downloaded from the RCSB PDB database (PDB ID: 6VXI) (Orlando & Liao, 2020). The 3D coordinates of 30 TH β C compounds were obtained from the literature and drawn using the Cresset software (Spindler et al., 2016). The aforementioned receptor and ligand molecules discussed in the following sections were used for the analysis. A graphical overview of the workflow followed in the paper is given in Figure 1.

2.2. Molecular alignment and 3D-QSAR modelling

The data set was divided into the training and test set molecules taken from the published article and aligned with the core structure drawn by the Cresset. The quality of molecular alignment is one of the crucial steps to perform significant 3D-QSAR modelling. To establish the field-based 3D-QSAR model, all optimized structures were loaded into the computational chemistry suite Forge v0.6.0, along with their associated biological activity. Out of thirty molecules, twenty-six (80%) were chosen at random as a training set to develop the model, and the remaining six compounds (20%) served as a test set to evaluate the model. The molecules were chosen for the training, and test sets encompass the entire range of biological activities (Floresta et al., 2018; Ahamad et al., 2018). In the training and test set molecules were aligned to the reference compound by maximum common substructure conformers with matching rules normal (element and hybridization) using a (by default) customized arrangement (Floresta et al., 2018). The eXtended Electron Distribution (XED) force field was used to produce field points (negative and positive electrostatic, van der Waals, and hydrophobic effects) of each molecule (Floresta et al., 2018). For building the 3D-QSAR model, default parameters such as the maximum number of components were set to 20, the sample point maximum distance was set to 1.0 Å, Y scrambles were set to 50. For overall similarity, Forge module of Cresset software was utilized, which uses 50% field

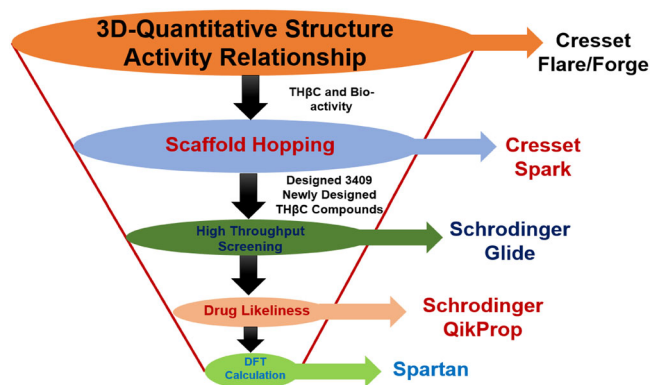


Figure 1. The workflow of the study: 3D-QSAR, scaffold hopping, molecular docking based high throughput screening, drug likeliness of RO5, ADMET, and DFT calculation techniques were applied in the current study.

similarity and 50% dice volume similarity. The overlays with the best matching low-energy conformations to the template were considered for building the 3D-QSAR model. The experimental activity (IC_{50}) of the data set compounds were converted to its logarithmic scale by using the formula: $pIC_{50} = -\log(IC_{50})$. The field point-based descriptors were utilized to generate a 3D-QSAR model (Spindler et al., 2016).

2.3. Homology modelling and validation

As mentioned earlier, the ABCG2 transporter resolved by cryo-electron microscopy 3D structure with a resolution of 3.70 Å (PDB code: 6VXI chains: A and B) was retrieved from the PDB database. We also retrieved the protein's FASTA sequence from UniProt (Q9UNQ0). While comparing the receptor molecule for missing data, we found few significant amino acid residues were missing from crystal structure. Therefore, to maintain the integrity of the study, we performed homology modelling to build the missing residues. We used the Prime-advanced homology modelling tool of Schrödinger to build the missing residues in the 3D structure of ABCG2 (Jackson et al., 2018).

2.4. Active site calculation and ligand molecules preparation

The ABCG2 four-digit PDB ID 6VXI was used as input to identify the active site, which gives significant insight into recognizing internal cavities, surface structural pockets, shape and volume of every pocket of the protein. The active site and the interactive residues were selected with the help of PDBsum and CASTp online tools (Laskowski et al., 1993; Tian et al., 2018). Furthermore, the ligand input zone comprises a sketcher that helps users draw, edit, and import the 2D structure. The ligands were prepared using Flare module v6.0.1 of Cresset software and the output files can be saved as .sdf, .pdb file format, which can be enabled in any visualization tool.

2.5. Scaffold hopping to designing of new molecules

All the 30 TH β C molecules were evaluated using Hoechst 33342 and Pheophorbide A assays for ABCG2, and the range of activities is wide enough to create an efficient model. Marvin sketch was executed to create the 2D chemical structures of all the molecules under consideration. With the help of MMFF94 force field molecular mechanics, energy minimization was performed. At the semi-empirical stage, the 3D geometrical structures of all the compounds were also optimized. The Forge module was used to measure the protonation state, assuming a pH of 7.0. The loaded molecules were displayed in the wizard with an option to control the score weighting used with one reference molecule in an editable form. Herein, multiple molecules were executed to make a chemical series (Floresta et al., 2019). Lastly, databases ChEMBL common, Zinc databases, VEHICLE (ring systems), and eMolecules have been used that act as building blocks for the corresponding R-group modification. An experimental setup was used that is required for the ND

molecules, and the calculations were performed. Spark v0.7.0 was used for the scaffold hopping technique.

2.6. Determination of ADMET properties

The ADMET properties of the top four ND-TH β C compounds, earlier synthesized compounds and the standard drug mitoxantrone from the library were selected to determine and evaluate drug-likeness by using the QikProp module of Schrödinger commercial software (Schrödinger, 2012; Ahamad et al., 2019). The analysis provides major physicochemical properties such as flexibility, molecular weight/size, hydrophobicity, bioavailability, FOSA, PISA, QPpolrz, QPlog, QPlogPC16, QPlogPoct, QPlogPw, QPlogSPo/w, QPloglogS, QPlogCaco, QPlogBB, and %HOA (Daina et al., 2017; Lee et al., 2003; Lipinski, 2016).

2.7. Binding free energy calculation (Prime/MM-GBSA)

The docked complexes were analyzed by MM-GBSA method. The OPLS2005 force field and VSGB 2.0 solvation model were employed for determining the post-binding energies for a set of receptor and ligands. The following equation was used for calculating the binding free energy:

$$\Delta G_{\text{Bind}} = \Delta G_{\text{complex}} - \Delta G_{\text{receptor}} - \Delta G_{\text{ligand}}$$

Where ΔG is the free energy for each complex, receptor, and ligand individually.

2.8. DFT calculations

The Spartan'20 package performed the DFT calculations with B3LYP/6-31G* basis set in the gas phase (Haque et al., 2018). The Spartan software was installed on a Tyrone workstation.

3. Results and discussion

3.1. ABCG2 3D structure modelling

The ABCG2 structure was modeled as PDB: 6VXI crystal structure, where amino acids at positions 47–60, 302–327, and 355–368 were missing. So that it is necessary to construct the 3D structure of ABCG2 with the help of the Prime-advanced homology modelling tool. Moreover, ABCG2 consists of 655 amino acids and comprises chains A and B. After the model generation, loop refinement was done where all the parameters were set to default, and out of five models, one of the best models was taken for further studies.

3.2. 3D-QSAR model and statistical analysis

Herein, we have developed the 3D-QSAR model of TH β C molecules that provide a global view to predict against the ABCG2 receptor. For this purpose, we have utilized 30 TH β C molecules gathered from the literature source and developed various models, but herein, one of the best model is discussed (Spindler et al., 2016). The division of molecules into training and test sets is an important step to build a

3D-QSAR model. Out of thirty molecules, six were selected for the test, and the remaining were in the training set, along with IC_{50} (biological activity) values of the corresponding molecules (Supplementary Table S1) (Spindler et al., 2016). The molecules were aligned on the core structure of TH β C, and showed a good alignment, as shown in (Figure 2A).

The division of training and test into subsets were created manually and tried splitting the molecules randomly. The correlation coefficient $r^2 = 0.99$, and good cross-validation regression coefficient values were $q^2 = 0.92$ estimated. The dataset was cross-validated with the training set and then we found that the model exhibited excellent predictive and descriptive capabilities. On the other hand, the test set calculated accurately cross-validated was found $r^2_{cv} = 0.32$. The fitness plot visualized the 3D-QSAR model, whereas the training set molecules were shown in blue data points and the test molecules were in purple (Figure 2B and Supplementary Figure S1). 3D-QSAR is one of the powerful statistical techniques that can provide the lead to design miraculous results in the generation of new molecules. The various substituents effect was generated, such as positive/negative electrostatic and steric contribution by red, cyan, and grey respective cube shape regions around the ligands. As well as favourable steric (dark green) and unfavourable steric (purple) regions around the ligands (Figure 2C). From such substitution effect, we found that the electron-withdrawing feature, hydrophobic features, hydrogen-bond donor, and negative/positive ionic features could be helpful to design new molecules. With these features' help, we took the best biological active molecule 27 that has IC_{50} 0.233 μ M value and then performed the Active Cliff Summary (Figure 2D).

3.3. Activity Atlas model visualization

Activity Atlas is a method for qualitatively and probabilistically analyzing the structure-activity relationship (SAR). Using the Activity Atlas, the SAR of a group of chemicals was calculated by accounting for their shape, electrostatic, steric, and hydrophobic characteristics. An overall qualitative perspective of the set of substances is presented by Activity Atlas using a Bayesian methodology. The Activity Atlas model produces the structural comprehension of the SAR of a chemical library (Attiq et al., 2022). We created an Activity Atlas model for activity from a training set of aligned TH β C compounds that were previously reported (Xing et al., 2022). The pIC_{50} values of the substances were used to build the Activity Atlas model. The chemicals exhibit biological activity where hydrophobic contact can either be advantageous or detrimental, as indicated by the colors green and magenta, respectively, in the 'Activity Cliff Summary of Hydrophobics' (Ahmad et al., 2022). Figure 2D shows the Activity Cliff Summary model for the active compound 27 of TH β C using the SAR mechanism of activity. Favourable hydrophobics are depicted in green, and unfavourable hydrophobics are displayed in magenta. At the same time, positive and negative electrostatic zones are represented in red and cyan, respectively, to illustrate the favourable and unfavourable locations for the improvement of biological activity.

3.4. Identification of field points and visualization

The TH β C derivatives demonstrated the 3D-QSAR model and the structural field point area controlling the predicted

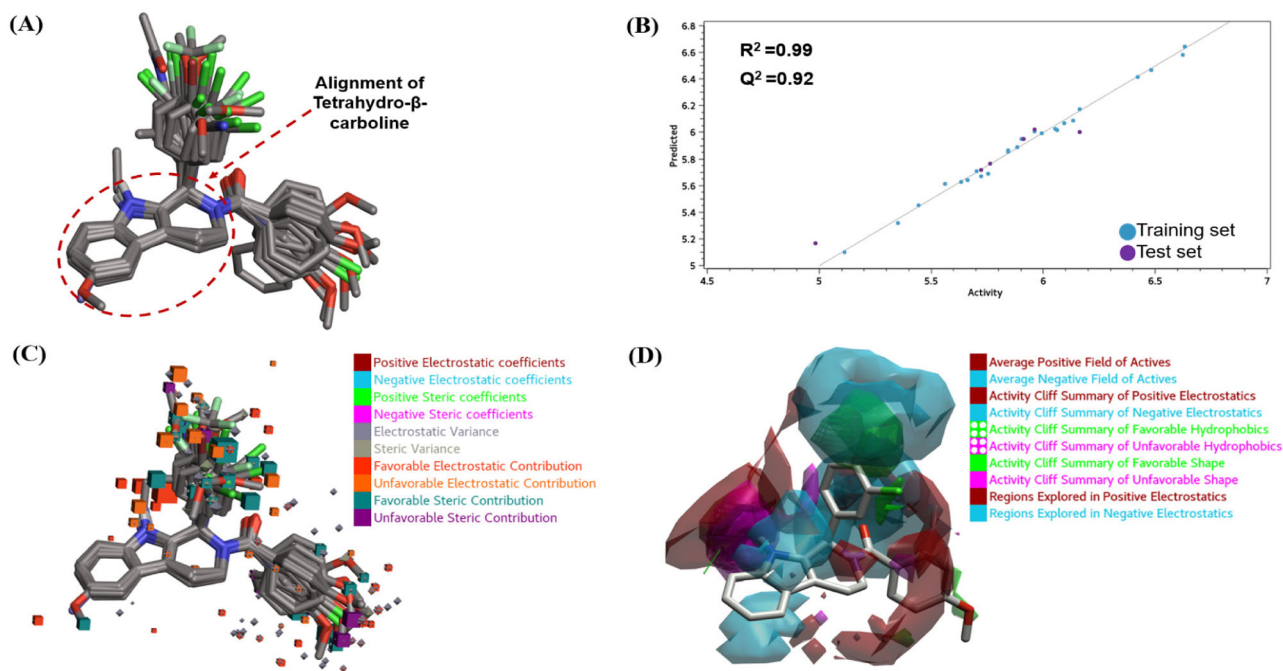


Figure 2. 3D-QSAR studies: (A) The alignment of 30 TH β C compounds utilized in QSAR model, (B) The fitness plot plotted between predicted and activity illustrated of training (blue color) and test set (purple color) molecules, (C) Molecular representation of aligned training and test set molecules with their respective molecular field points depicted as cube shapes showing the summary of electrostatics coefficient, steric coefficient, electrostatic variance, steric variance, favourable and unfavourable electrostatic region of the best biological active molecule, (D) Compound 27 activity cliff summary model for the active chemicals of TH β C using the SAR mechanism of activity. Favourable hydrophobics are depicted in green, and unfavourable hydrophobics are depicted in magenta, while positive and negative electrostatic zones are represented in red and cyan, respectively.

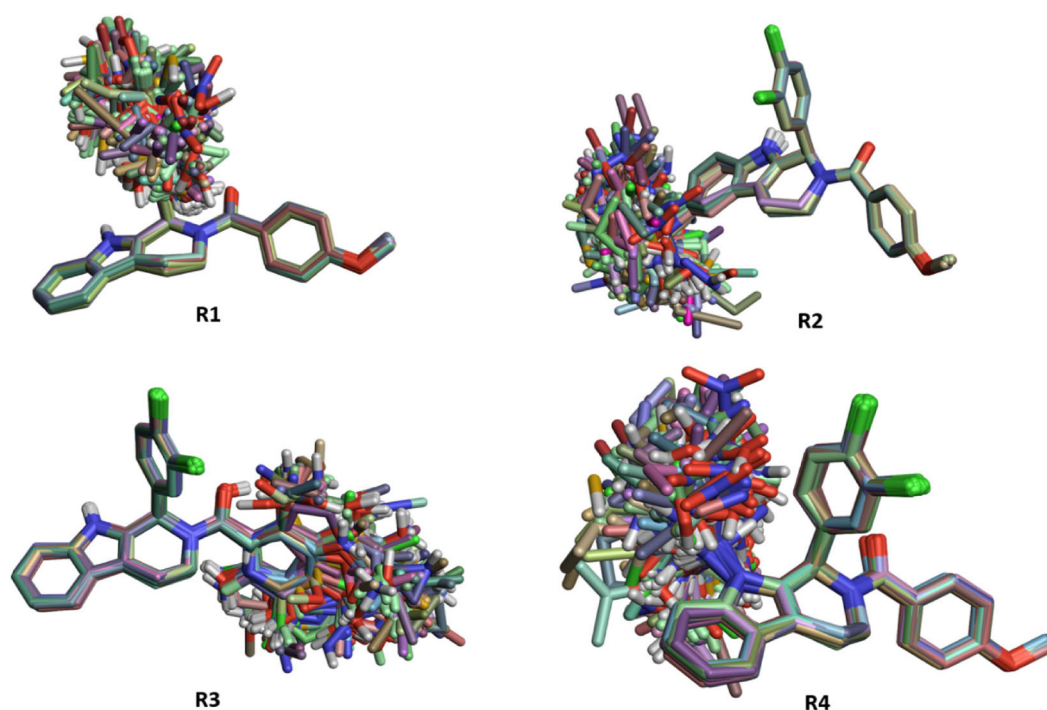


Figure 3. Scaffold hopping illustrated the generated newly designed molecules and alignment on the earlier compound 27 in different frame modifications at position substituted R1, R2, R3 and, R4 (A-D), a total of 3409 molecules, respectively.

activity. The localization of the space field point capture and 3D-QSAR model field points were superposed onto the reference molecule. To understand the SAR process of TH β C compounds via the 3D-QSAR model. The model showed local fields which dictate the impact on the biological activity of the compound could increase or decrease, which means the more significant the connection of the electrostatic/steric fields, then the larger will be the field points, and it could affect the affinity values that will be increase/decrease. The positive steric coefficient, which revealed a steric bulkiness leading to higher activity was a good predictor to recognized 3D-QSAR model. The positive and negative electrostatic coefficients influence the activity of substituents. Furthermore, shape and hydrophobic field points are associated with high biological activity that could suggest new molecules with positive (red) or negative (cyan) fields. Similarly, electrostatics positive (green) denote favourable contributions through an increased electrostatic field, and electrostatics negative (orange) correspond to unfavourable electrostatic contributions, illustrating a decrease in the model's predicted activity (Figure 2C).

3.5. Designing of new molecules via scaffold-hopping

The objective of the scaffold-hopping is to understand the electrostatic field points and steric hindrance. These are caused in the molecules by the introduction of certain groups, which in turn affect the biological efficacy. Electrostatic field points (positive value) are produced by the insertion of electron-donating groups in the molecules such as -OH, -NH₂, R-NH₂, and halogens except for fluorine.

However, the electrostatic field points (negative value) are produced by alkyl groups such as methyl, ethyl, primary,

secondary, and tertiary alkyl groups. The bulky groups and phenyl rings cause steric hindrance. It is a well-known fact that polar groups enhance the hydrophilicity (water solubility) and non-polar groups like alkyl groups and phenyl rings produce lipophilicity. Therefore, drug candidature must be water soluble and lipid soluble. So, in view of these points, we herein evaluated the electrostatic field points of indole-bearing tetrahydropyridine derivatives by substituting R1, R2, R3, and, R4 groups, targeting ABCG2 protein (as shown in Figure 3).

In the present study, the electrostatic field points (positive value as shown in red color) are produced in ND-TH β C1 by the incorporation of ethanolic group (-CH₂-CH₂OH) at para position of (phenyl ether) of tetrahydropyridine ring, which in turn enhance the polar interaction (Figure 4A). In the case of compound ND-TH β C2, the positive value as presented in red color is increased by the insertion of a methoxy group at para position of the phenyl ring of tetrahydropyridine and -OH group present at the alkyl chain of the benzene ring of basic indole core structure also enhances the positive field points. Conversely, negative field points (as shown in cyan color) are caused by the presence of an alkyl chain of the benzene ring of indole (Figure 4B). In compound ND-TH β C3, positive values were produced by the insertion of polar groups -OH at ortho position and alkoxy group at the para position of the benzene ring of tetrahydropyridine (Figure 4C). Finally, in compound ND-TH β C4, strong electrostatic field points (positive values) were observed on diamine methyl amine salt substitution at the nitrogen of indole ring, which appreciably increased the polar character within the molecule and resulted in polar interaction (Figure 4D).

In detail, the core TH β C of compound 27 (1-(3,4-dichlorophenyl)-2-(4-methoxybenzoyl)-1H,2H,3H,4H,4aH,9H,9aH-pyrido

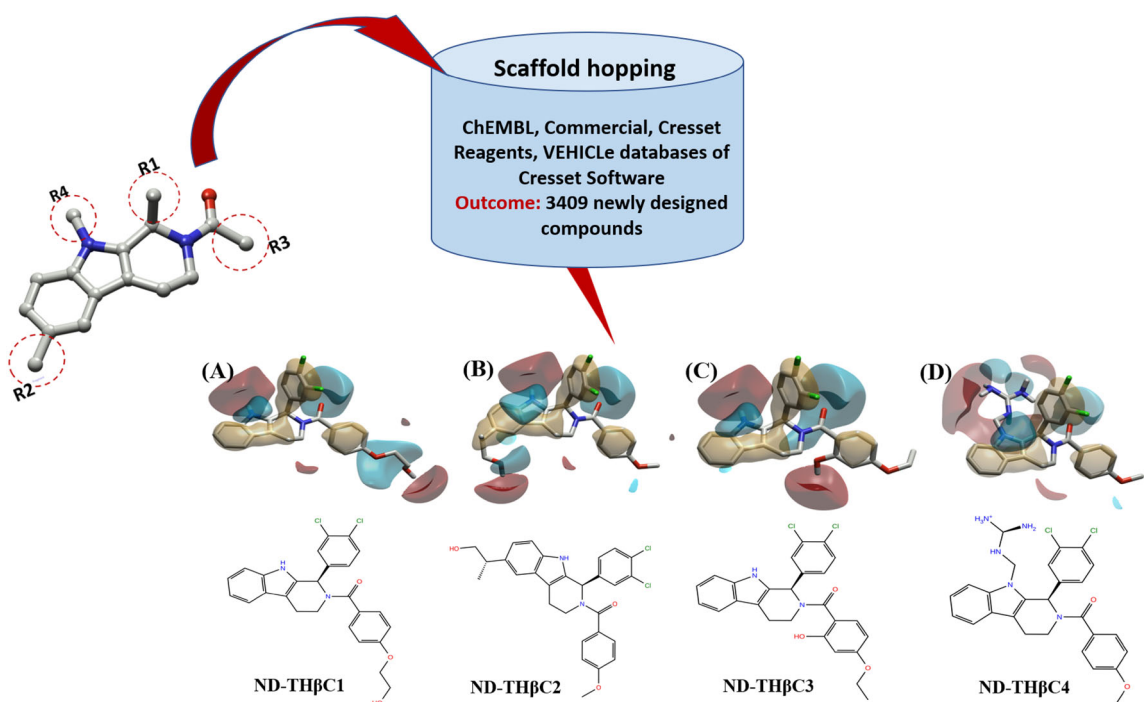


Figure 4. The scaffold hopping results of ND-TH β C1 to ND-TH β C4 molecules illustrate electrostatic, steric, and van der Waals field effects from A-D and 2D plots, respectively.

[3,4-b] indole), bearing versatile functional groups is an ABCG2 inhibitor. The field effect that appeared on compound 27 showed steric, electrostatic, and, hydrophobic (Supplementary Figure S2). In order to explore its inhibitory activity against ABCG2 proteins, new molecules have been designed by different substitution R1, R2, R3, and, R4 groups on the core structure of compound 27. TH β C is a heterocyclic compound ending with indole ring and tetrahydropyridine ring and has been reported as a potential inhibitor by blocking ABCG2 protein in MDR (Spindler et al., 2016). It was observed that a halogen substitution at the meta or para position in the phenyl ring compared to the ortho position was found to be a highly potent compound with inhibitory activity in the sub-micromolar range. Compound 27 (IC₅₀ = 0.233 μ M) with a para-methoxy phenyl group showed high efficacy compared to unsubstituted compounds (Figure 3) (Moinul et al., 2022).

A list of potent structural features has been prepared by substitutions that might be considered better ABCG2 inhibitors and have been evaluated (Figure 3). More significant or more extensive field regions strongly correlate with inhibitory activity. The electrostatic potential of the molecule has been presented in different colors. The red color region indicates the positive values of the electrostatic potential; however, cyan color indicates the negative values of the potential. The golden color represents lipophilicity that is increased in the molecule by substituting alkyl groups and aryl groups such as methyl, ethyl, propyl, and benzene ring (Figure 4). It is well-known that the greater the field points, the greater the electrostatic fields/steric hindrance (Figure 4).

The ND-TH β C1 molecule was designed by R3-substitution at para position of the benzene ring (-OH). Electron donating group (-OH) contributed positive field points and formed

hydrogen bonds with ABCG2 protein of chain A. It was observed that the electrostatic field points were enhanced by R3 substitution, which was represented by red color (positive field) and cyan color (negative field). These enhanced electrostatic field points were responsible for stable interaction with the target. The -OH group interact with uncharged polar residues Gln437, Asn436, and Thr439 of ABCG2 of chain A. It was also found that pi-pi stacking interaction took place when substituted by the R1 group at the benzene ring of tetrahydropyridine. This led to the interaction with a polar residue Thr439 of ABCG2. π - π stacking interactions are much weaker but play a vital role. The resulting model simultaneously displays molecular size and shape and electrostatic potential value (Figures 4A and 5C).

The ND-TH β C2 molecule, R2 substitution at para position made to carry out by methoxy group (3'-methyl, proethoxy), the group comprises of atom oxygen which is electronegative in character but due to the presence of two lone pairs methoxy group acts as a strong electron releasing group. Hence, it created electrostatic solid positive field points represented by red color and weak electronegative field points. The positive field points support the formation of hydrogen bonds between -OH group and Glu446 residue of the ABCG2 protein of chain B. Here we focus on the field effect on the reaction of glutamic acid (Glu) with -OH group. Glu is more vulnerable to oxidative attack by the -OH group. The polar and uncharged (hydrophilic) amino acids can make hydrogen bonds with water and are usually more soluble than the non-polar amino acids. In the case of ND-TH β C2, it was observed that negative field points (cyan color) are produced around pyrrole group at position R4. Also, pyrrole-based scaffolds were employed to develop anti-tumor agents acting on the gene (Figures 4B and 5D) (Gribble, 1996).

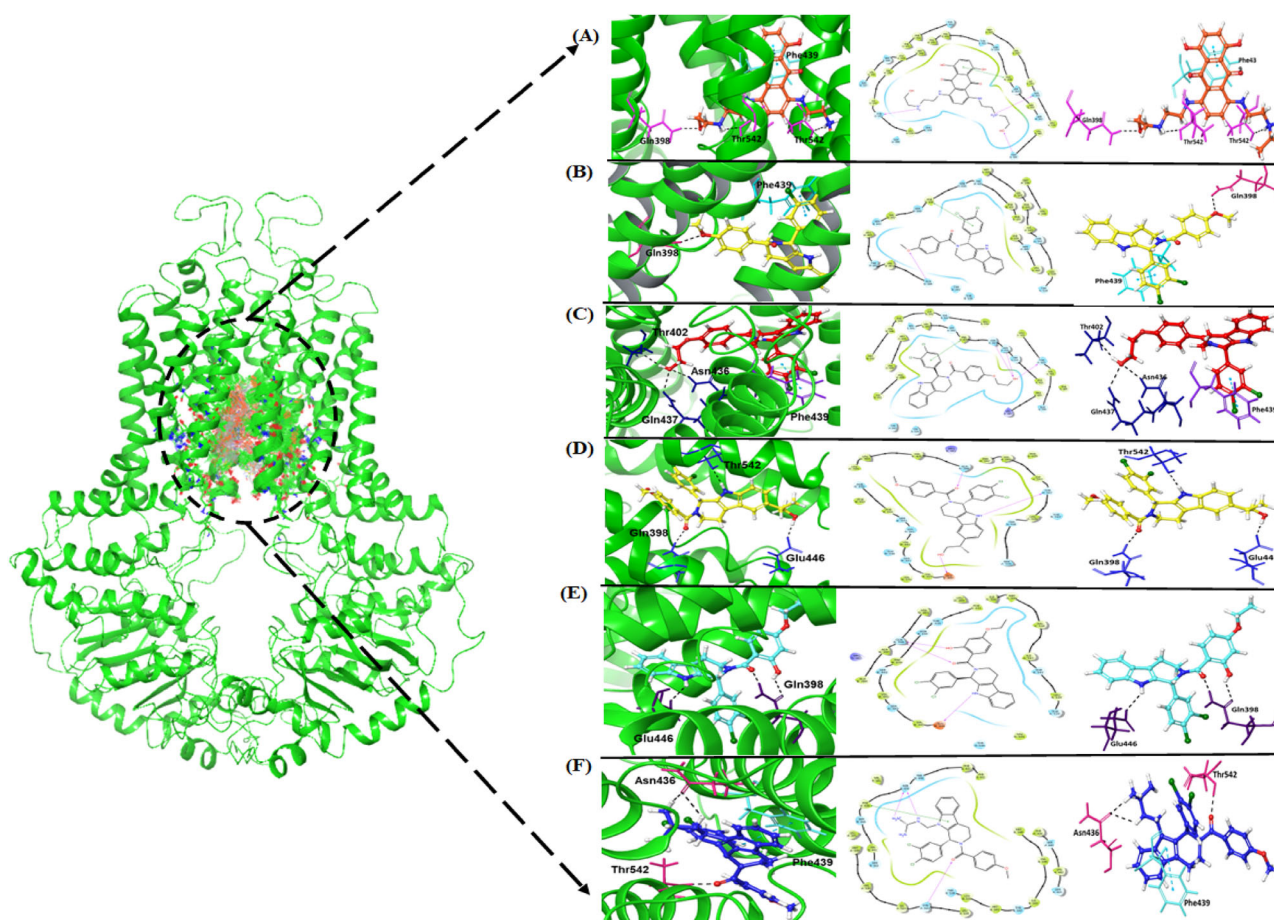


Figure 5. Elucidation of 3D interaction plots of the molecular docking studies to illustrate the interactive residues by H-bonds and 2D plot of the H-bonds interaction showed by the pink arrow and hydrophobic residues of ABCG2 at the binding cleft of mitoxantrone, compound 27 and ND-TH β C1-4 (A-F) respectively.

The ND-TH β C3 molecule has been designed by substituting the R3 (ethoxy) group at the ortho position of the benzene ring of ND-TH β C3. This group is a better electron-donating group and displays strong positive electrostatic field points, as represented in red color (Figures 4C and 5E). Finally, the ND-TH β C4 molecule was designed by R4 substitution at the nitrogen of indole moiety. This substituting R4 comprises of diamino methyl amino group. Three nitrogen atoms are present in this group: electron donating groups. Due to the presence of nitrogen atoms, strong electrostatic positive field points are observed. This led to the formation of polar interaction (Figures 4D and 5F).

3.6. Molecular docking based virtual screening

Molecular docking was carried out to predict the best-preferred interaction between ligand and receptor which bound to one another by the H-bond and π - π interaction, as well as supported by hydrophobic residues to make the complex stable (Figure 5). Herein, Schrödinger's Glide module was utilized with 30 earlier synthesized and 3409 newly designed TH β C molecules with ABCG2 receptor at the binding cleft to identify the potent hit molecules (Supplementary Table S2). To understand the binding pose interaction pattern and binding scores, the mitoxantrone drug was analyzed and found the three H-bond interactions Gln398, Thr542 of chain

B, and Thr542 of chain A of ABCG2 and the binding XP GScore was -8.162 kcal/mol. The complex provided stability via several van der Waal's interactions Gln398, Val401, Phe431, Phe431, Phe432, Phe432, Thr435, Thr435, Asn436, Phe439, Phe439, Ser440, Ser440, Val442, Val442, Ser443, Ser443, Thr538, Leu539, Leu539, Ile543, Ile543, Val546, Val546, Met549, Met549, and IFD score was noted as -2390.35 kcal/mol (Figure 5A and Table 1). We also estimated the MM-GBSA value of the mitoxantrone and ABCG2 complex to be -80.51 kcal/mol. The best active compound 27 from the earlier synthesized library interacted with one H-bond Gln398 of chain B of ABCG2, and ABCG2 was a stable complex along with several hydrophobic residues Val401, Thr402, Leu405, Phe431, Phe432, Thr435, Asn436, Phe439, Phe439, Ser440, Ser440, Val442, Val442, Ser443, Thr538, Thr538, Leu539, Thr542, Thr542, Ile543, Phe545, Val546, Val546, Met549, and Met549 and provided XP GScore -8.225 kcal/mol as well as IFD score -2396.56 kcal/mol as shown in (Figure 5B and Table 1). The calculated MM-GBSA value of the compound 27 and ABCG2 complex is -86.67 kcal/mol, which is relatively better than the mitoxantrone drug.

The docking result of ND-TH β C1 binds tightly at the binding cleft of the ABCG2 receptor and forms three H-bonds Thr402, Asn436, and Gln437 residues of chain A and forming stable confirmations. One of the potent molecules formed hydrophobic interactions with residues Gln398, Val401,

Table 1. The table illustrated that the compound name, smiles, H-bonding interacting residues, number of H-bonds, hydrophobic residues, docking XP GScore, IFD scores, and ΔG through MM-GBSA approach of the drug mitoxantrone, compound 27, and ND-TH β C1 to ND-TH β C4.

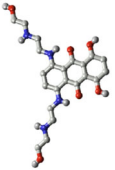
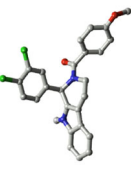
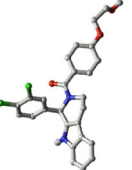
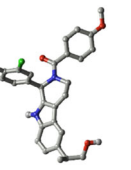
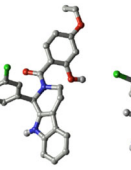
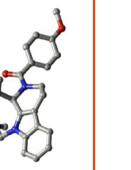
Compounds S. No	Smiles	Chemical structure	H-bond residues	Hydrophobic interactive residues	XP GScore	IFD (kcal/mol)	No. of H-bond	MM-GBSA (kcal/mol)
Mitoxantrone	<chem>O=C1c2c(NCCNCCO)ccc2NCCNCCO1C(=O)c2c1c(O)ccc2O</chem>		Gln398, Thr542 and Thr542	Gln398, Val401, Phe431, Phe432, Phe432, Thr435, Thr435, Asn436, Phe439, Phe439, Phe440, Ser440, Val442, Val442, Val442, Ser443, Ser443, Thr538, Leu539, Leu539, Ile543, Ile543, Val546, Val546, Met549, and Met549	-8.162	-2390.35	3	-80.51
Compound 27	<chem>Clc1c(Cl)ccc1C@H]2c3c(c4cccc4)hH]3CCN2C(=O)c5ccc(O)c5)c1</chem>		Gln398	Val401, Thr402, Leu405, Phe431, Phe432, Thr435, Asn436, Phe439, Phe439, Ser440, Ser440, Val442, Val442, Ser443, Thr538, Thr538, Leu539, Thr542, Thr542, Ile543, Phe545, Val546, Val546, Met549, and Met549	-8.225	-2396.56	1	-86.67
ND-TH β C1	<chem>Fm-c(ccc1OCCO)cc1</chem>		Thr402, Asn436 and Gln437	Gln398, Val401, Leu405, Phe432, Thr435, Phe439, Phe439, Ser440, Val442, Val442, Ser443, Arg482, Pro485, Phe489, Thr538, Leu539, Thr542, Thr542, Ile543, Phe545, Val546, Val546, Met549, and Met549	-10.336	-2399.95	3	-96.88
ND-TH β C2	<chem>FmC(O)CO</chem>		Gln398, Glu446, and Thr542	Val401, Val404, Leu405, Phe432, Asn436, Phe439, Phe439, Ser440, Ser441, Val442, Ser443, Val445, Arg482, Val534, Ser535, Thr538, Thr538, Leu539, Thr542, Ile543, Val546, and Phe547	-9.734	-2399.15	3	-98.52
ND-TH β C3	<chem>Fm-c(ccc1OCCO)c(O)c1</chem>		Gln398, and Glu446	Ala394, Ala397, Val401, Leu405, Phe432, Thr435, Asn436, Phe439, Ser440, Val442, Ser443, Val445, Arg482, Val534, Thr538, Thr538, Leu539, Thr542, Ile543, Val546, Met549, and Ile550	-9.846	-2397.49	2	-97.53
ND-TH β C4	<chem>FmCNC(N)N</chem>		Asn436 and Thr542	Val401, Leu405, Phe431, Phe432, Thr435, Phe439, Phe439, Ser440, Ser440, Val442, Val442, Ser443, Ser443, Thr538, Leu539, Leu539, Met541, Thr542, Ile543, Ile543, Val546, Val546, Met549, and Met549	-9.992	-2395.27	2	-94.90

Table 2. The drug likeliness properties of the drug mitoxantrone, compound 27, and newly designed compounds ND-TH β C1 to ND-TH β C4.

Compounds S. No	TPSA	SlogP	Rotatable bonds	CNS	MW	Dipole	SASA	WPSA	Volume	DonorHB	AccptHB	XP GScore	RO5
Mitoxantrone	163.18	3	16	-2	444.486	7.96	776.201	0	1377.38	4	9.9	-8.162	1
Compound 27	45.3	6.3	4	1	451.4	6.203	709.964	128.687	1285.599	1	3.75	-8.225	1
ND-TH β C1	66	6.1	7	0	481.377	3.577	750.511	129.757	1368.004	2	5.45	-10.336	1
ND-TH β C2	66	6.8	7	0	509.431	6.606	804.069	129.398	1474.395	2	5.45	-9.734	2
ND-TH β C3	66	6.4	6	0	481.377	6.92	754.147	129.552	1376.861	1	3.5	-9.846	1
ND-TH β C4	95	5.7	6	1	524.449	5.09	753.502	105.917	1434.429	5	7.25	-9.992	1

Table 3. The ADMET properties of the drug mitoxantrone, compound 27, and newly designed compounds ND-TH β C1 to ND-TH β C4.

Compounds S.No.	FOSA	PISA	QPpolrz	QPlog PC16	QPlog Poct	QPlog Pw	QPlog Po/w	QPlogS	CIQP logS	QPlog HERG	QPlog BB	QPlog Kp	QPlog Khsa	%HOA
Mitoxantrone	305.758	168.39	40.303	15.415	25.245	16.86	0.444	-1.642	-2.932	-7.488	-2.989	-9.082	-0.344	15.25
Compound 27	163.661	377.02	47.612	14.269	20.181	9.03	6.442	-8.069	-8.221	-6.479	0.342	-0.747	1.306	100
ND-TH β C1	149.809	372.033	48.936	15.683	22.896	11.969	5.668	-7.561	-8.053	-6.638	-0.465	-1.552	0.995	100
ND-TH β C2	294.038	290.992	52.42	16.105	24.178	11.483	6.299	-8.506	-8.627	-6.494	-0.405	-1.666	1.274	94.217
ND-TH β C3	201.489	343.527	49.66	15.201	20.883	8.487	6.825	-8.652	-8.949	-6.509	-0.202	-1.392	1.525	100
ND-TH β C4	197.043	334.162	49.948	16.575	28.672	17.554	2.986	-2.506	-4.736	-8.276	0.034	-5.94	0.555	50.856

Minimal Ranges: MW = Molecular Weight (130.0/725.0), accPthB = Acceptor - Hydrogen Bonds (2.0/20.0), rotor = No. of Rotatable Bonds (0.0/15.0), logP o/w = log P for octanol/water (-2.0/6.5), dipole = Dipole Moment (1.0/12.5), logS = log S for aqueous solubility (-6.5/0.5), SASA = Total solvent accessible surface area (300.0/1000.0), ClogS = log S - conformation independent (-6.5/0.5), FOSA = Hydrophobic solvent accessible surface area (0.0/750.0), logBB = log BB for brain/blood (-3.0/1.2), FISA = Hydrophilic solvent accessible surface area (7.0/700.0), log Kp = log Kp for skin permeability (Kp in cm/hr), PISA = Carbon Pi solvent accessible surface area (0.0/450.0), log Khsa = log Khsa Serum Protein Binding (-1.5/1.5), WPSA = Weakly Polar solvent accessible surface area (0.0/175.0), Lipinski Rule of 5 Violations-RO5 (maximum is 4), PSA = vdW Polar surface area (7.0/200.0), % Human Oral Absorption in GI (\pm 20%) (<25% is poor), volume = Molecular Volume (A³) (500.0/2000.0), Apparent Caco-2 Permeability (nm/sec) (<25 poor, >500 great), donorHB = Donor - Hydrogen Bonds (0.0/6.0), Apparent MDCK Permeability (nm/sec) (<25 poor, >500 great), CNS (-5.00/3.00).

Leu405, Phe432, Thr435, Phe439, Phe439, Ser440, Val442, Val442, Ser443, Arg482, Pro485, Phe489, Thr538, Leu539, Thr542, Thr542, Ile543, Phe545, Val546, Val546, Met549 and Met549 are seen in the centroid region along with lowest XP GScore -10.336 kcal/mol and IFD score -2399.95 kcal/mol (Figure 5C and Table 1). The MM-GBSA free energy estimated for the ND-TH β C1 and ABCG2 is -96.88 kcal/mol at the active site. The docking results revealed the molecules' binding potency, active pose, and mechanism of action.

Similarly, it was observed that the complex of ND-TH β C2 and ABCG2 interacted at the binding cleft and formed stable conformation that revealed three H-bond with residues Gln398 and Glu446 of chain B and Thr542 residue of chain A along with several van der Waal interactions involved such as Val401, Val404, Leu405, Phe432, Asn436, Phe439, Phe439, Ser440, Ser441, Val442, Ser443, Val445, Arg482, Val534, Ser535, Thr538, Thr538, Leu539, Thr542, Ile543, Val546 and Phe547 that showed strong interactions with residues and XP GScore found to be -9.734 kcal/mol and IFD score -2399.15 kcal/mol (Figure 5D and Table 1). After docking energy calculation, the MM-GBSA of the complex ND-TH β C2 and ABCG2 was -98.52 kcal/mol, which is comparatively higher than each complex.

The complex of ND-TH β C3 strengthened for the formation of the good binding orientation of two H-bonds with the Gln398 and Glu446 amino acid residues of chain B of ABCG2. The complex provides stable conformation with various van der Waal interactions participated Ala394, Ala397, Val401, Leu405, Phe432, Thr435, Asn436, Phe439, Ser440, Val442, Ser443, Val445, Arg482, Val534, Thr538, Thr538, Leu539, Thr542, Ile543, Val546, Met549, and Ile550 residues and the XP GScore -9.846 kcal/mol and IFD score -2397.49 kcal/mol (Figure 5E and Table 1). The MM-GBSA of the complex ND-

TH β C3 and ABCG2 was -97.53 kcal/mol. Since the docking poses adequately formed a stable complex with ND-TH β C4, which renders the two H-bonds Asn436 of chain B and Thr542 residue of chain A and induced the molecule significantly. Apart from H-bond formation, the van der Waal residues Val401, Leu405, Phe431, Phe432, Thr435, Phe439, Phe439, Ser440, Ser440, Val442, Val442, Ser443, Ser443, Thr538, Leu539, Leu539, Met541, Thr542, Ile543, Ile543, Val546, Val546, Met549, and Met549 and provided XP GScore to be -9.992 kcal/mol, whereas the IFD score -2395.27 kcal/mol (Figure 5F and Table 1). The post-docking energy calculation of MM-GBSA was -94.90 kcal/mol for the complex ND-TH β C4 and ABCG2, which indicates stable conformation of the molecule. Additionally, a 2D diagram was generated to reveal the same molecular interactions. The findings rendered a molecular-level understanding to infer that the proposed compounds ND-TH β C1 to ND-TH β C4 are promiscuous and could probably act as potential antagonists toward the active groove of ABCG2.

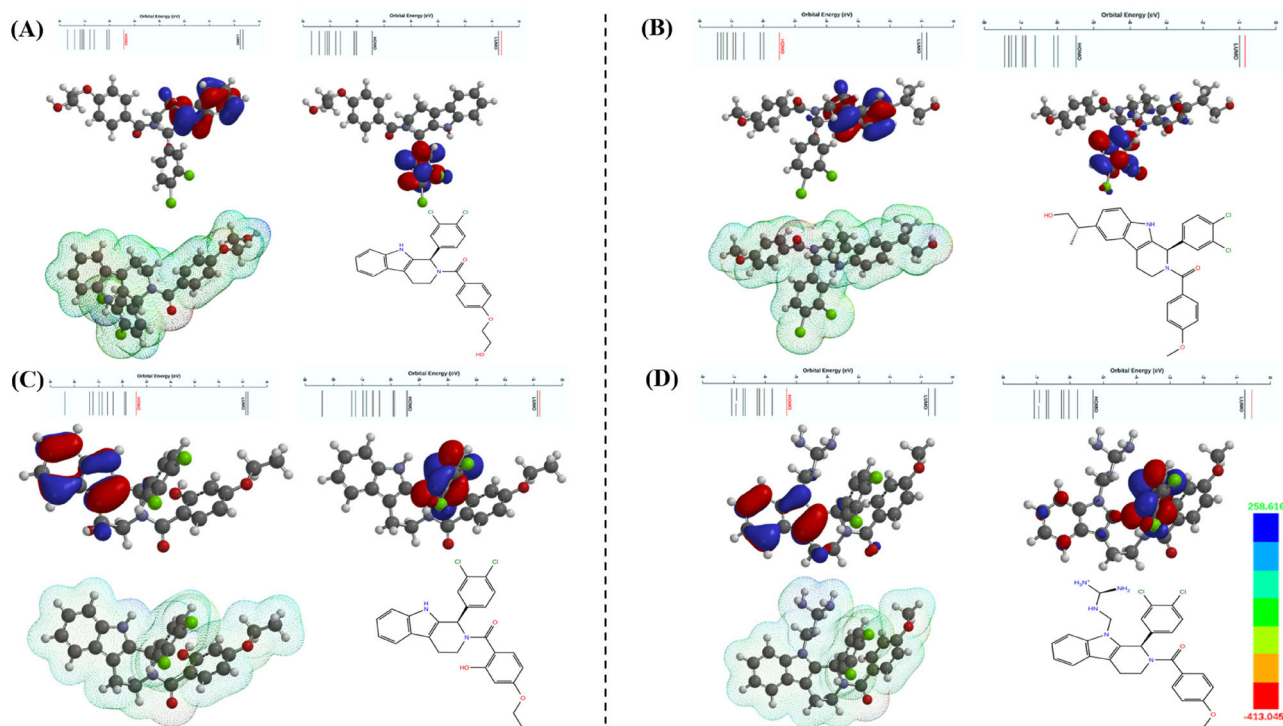
3.7. Drug likeliness and ADMET properties

ADMET and pharmacological properties are crucial for selecting and developing drug candidates. Therefore, the screened compounds were investigated for ADMET based on RO5 properties. For this purpose, the QikProp module was utilized, and the output of reported molecules had no violation of pharmacological properties for the four compounds, namely drug mitoxantrone, compound 27, and newly designed compounds ND-TH β C1 to ND-TH β C4 with blood-brain barrier penetration (-1.244 to 0.099), logP range from (-0.077 to 3.332), QPlogKhsa (-0.3 to -1.7), SASA (528 to 610), log Kp. The results revealed that the compounds were

Table 4. Calculated chemical reactivity parameters.

Compounds	E_{HOMO} (eV)	E_{LUMO} (eV)	ΔE^a (eV)	I^b (eV)	A^c (eV)	χ^d (eV)	η^e (eV)	σ^f (eV ⁻¹)	μ^g (eV)	ω^h (eV)
Mitoxantrone	-5.46	-1.14	0.32	0.46	0.14	0.30	0.16	3.12	-0.30	2.81
Compound 27	-5.40	-0.77	4.63	5.40	0.77	3.08	2.31	0.21	-3.08	2.05
ND-TH β C1	-5.49	-1.00	4.49	5.49	1.00	3.24	2.24	0.22	-3.24	2.34
ND-TH β C2	-5.43	-0.77	4.66	5.43	0.77	3.10	2.33	0.21	-3.10	2.06
ND-TH β C3	-5.45	-0.99	4.46	5.45	0.99	3.22	2.23	0.22	-3.22	2.33
ND-TH β C4	-5.41	-0.79	4.62	5.41	0.79	3.10	2.31	0.22	-3.10	2.08

$a = |E_{\text{HOMO}} - E_{\text{LUMO}}|$; $b = -E_{\text{HOMO}}$; $c = -E_{\text{LUMO}}$; $d = (I + A)/2$; $e = (I - A)/2$; $f = 1/2\eta$; $g = -(I + A)/2$; $h = \mu^2/2\eta$

**Figure 6.** Frontier orbitals and electrostatic potential map of ND-TH β C1 to ND-TH β C4 and respective 2D chemical structure of the compound.

within the acceptable range, indicating they possess high bioavailability and likeliness to be lead-like compounds (Tables 2 and 3) (Lee et al., 2003; Lipinski, 2016).

Lipinski rule violation: The compounds were further examined for the Lipinski RO5 parameters, including molecular weight (MW) less than 500, hydrogen bond acceptor (AccptHB) not more than 10, hydrogen bond donor (DonorHB) not more than 5, surface polar atoms not greater than 150 and the calculated octanol-water partition coefficient Clog P does not exceed 5 (Lipinski, 2016, Ahamad et al., 2021). The values for the mentioned parameters were estimated to look for the presence of drug-like properties. Out of all, the drug mitoxantrone, compound 27, and newly designed compounds ND-TH β C1 to ND-TH β C3 fitted with the Lipinski's properties except ND-TH β C4, all of them exhibited drug-likeness thereby having good absorption in the biological systems (Table 2).

3.8. DFT studies

Using DFT calculations, one can underpin and predict the interactions taking place at the supramolecular level as well as the stability and reactivity of a given system. It should be noted that the energy difference between the highest

occupied molecular orbital (HOMO) and lowest unoccupied molecular orbital (LUMO), commonly known as the band gap (ΔE), is the function of stability, reactivity, charge transfer, and many other photo-physical and electrochemical properties (Faizi et al., 2018; Mushtaque et al., 2017). Whereas a low ΔE value indicates higher chemical reactivity and is helpful for opto-electronic applications (Haque et al., 2018; Haque et al., 2019), a large ΔE value is correlated with higher stability. In this study, we performed DFT at the B3LYP level to determine global reactivity parameters (GRP) and other features. Both screened, and standard compounds were studied to correlate predicted activity with the structural features, and the results are summarized (Table 4 and Figure 6, Supplementary Figure S3). As can be seen, the HOMO of all the screened compounds lies in the range of -5.40 to -5.49 eV, which is close to the standard mitoxantrone (-5.46 eV).

On the other hand, LUMO level varied between -0.77 to -1.0 eV (-1.14 eV for mitoxantrone), yielding $\Delta E = 4.46$ - 4.66 eV. This value is typical for compounds with moderate stability, reactivity, and polarizability (Alshammari et al., 2021). An exciting feature of this study is the differences in the distribution of frontier orbital, especially HOMO. It is noted that HOMO resides over (4-(2-hydroxyethoxy)phenyl)methanone in

ND-TH β C1 while (4-methoxyphenyl)methanone in ND-TH β C2. Contrarily, HOMO was localised over indole fragment of the molecule in the case of ND-TH β C3 and ND-TH β C4 (Figure 6A–D). In all cases, LUMO was distributed over 3,4-dichlorophenyl fragment of the molecule, like compound 27 (Supplementary Figure S3). We also calculated GRPs, including ionization energy (I.E), electron affinity (E.A), electronegativity (χ), chemical potential (μ), chemical hardness (η), softness (σ), and electrophilicity index (ω) using the values of frontier energy levels (HOMO/LUMO energy levels). The value of η for all compounds is quite high (> 2), indicating good strength, stability, and comparison to the standard drug. The negative μ values also supplement this fact. The molecular electrostatic potential (MEP) map reveals charge density and reactive (electrophilic & nucleophilic) sites present over a molecule. Whereas the areas highlighted in blue are preferred sites for nucleophiles, those colored in red is attacked by electrophiles. The negative (red and yellow region) and positive (blue region) electrostatic potentials are localized according to the nature of the electro-negativity of atoms in the molecule.

4. Conclusion

Multi-drug resistance is one of the challenges in cancer chemotherapy, especially in breast cancer. Drug discovery of newer lead molecules is an urgent need to tackle such resistance as early as possible. The TH β C compounds have been found to show high activity against ABCG2-induced MDR cases. In this study, we performed a set of computational studies such as 3D-QSAR, scaffold hopping, molecular docking, IFD, MM-GBSA, and DFT analysis to design novel inhibitors. The 3D-QSAR study of TH β C compounds showed that the model has good correlation coefficient ($r^2 = 0.99$) and cross-validation regression coefficient ($q^2 = 0.92$) values. Molecular docking results showed that the newly designed compound ND-TH β C1 to ND-TH β C4 has a higher binding affinity and a more significant number of hydrogen bond interactions than the standard mitoxantrone drug and earlier synthesized compound. Furthermore, all four short-listed molecules showed comparatively similar HOMO levels with a slight variation in LUMO energy that signifies that the molecules are stable. Based on the analysis, our computational studies concluded that the newly designed molecules ND-TH β C1 to ND-TH β C4 were found to be more potent. These findings may help in the designing of new TH β C compounds for ABCG2. However, further *in vivo*, and *in vitro* validation is needed.

Acknowledgements

SA is thankful to IFTM University, Jamia Millia Islamia and Translational Bioinformatics Group, International Centre for Genetic Engineering and Biotechnology for providing the working environment and excellent infrastructure to pursue the doctoral research work.

Disclosure statement

None of the authors have conflicts and declare no competing interests.

Funding

The author(s) reported there is no funding associated with the work featured in this article.

ORCID

Shahnawaz Ahmad  <http://orcid.org/0000-0001-9039-3757>

Authors' contributions

SA contributed to extensive *in-silico* exercises, 3D-QSAR, molecular docking, MM-GBSA, scaffold hopping and DFT investigations, and original draft write-up in the manuscript. DG contributed major inputs, review, and corrections in the manuscript. TA contributed to reviews, and corrections in the manuscript. AI contributed to the final review, correspondence, and corrections in the manuscript.

References

- Ahamad, S., Hassan, M., & Dwivedi, N. (2018). *Designing of phenol-based β - carbonic anhydrase1 inhibitors through QSAR, molecular docking, and MD simulation approach*. 3 *Biotech*, 8(5), 1–18. <https://doi.org/10.1007/s13205-018-1278-z>
- Ahamad, S., Islam, A., Ahmad, F., Dwivedi, N., & Hassan, M. I. (2019). *2/3D-QSAR, molecular docking and MD simulation studies of FtsZ protein targeting benzimidazoles derivatives*. *Computational Biology and Chemistry*, 78, 398–413.
- Ahamad, S., Kanipakam, H., Birla, S., Ali, M. S., & Gupta, D. (2021). *Screening Malaria-box compounds to identify potential inhibitors against SARS-CoV-2 Mpro, using molecular docking and dynamics simulation studies*. *European Journal of Pharmacology*, 890, 173664.
- Ahamad, S., Hassan, M. I., Gupta, D., Dwivedi, N., & Islam, A. (2022). *Design and evaluation of pyrimidine derivatives as potent inhibitors of ABCG2, a breast cancer resistance protein*. 3 *Biotech*, 12(9), 1–17. <https://doi.org/10.1007/s13205-022-03231-1>
- Alshammari, M. M., et al. (2021). *Synthesis, characterization, anticancer and in silico studies of a pyrazole-tethered thiazolidine-2, 4-dione derivative*. *Journal of Biomolecular Structure and Dynamics*, 40(23), 13075–13082.
- Amaro, R. E., Baudry, J., Chodera, J., Demir, Ö., McCammon, J. A., Miao, Y., & Smith, J. C. (2018). *Ensemble docking in drug discovery*. *Biophysical Journal*, 114(10), 2271–2278.
- Arnold, M., Morgan, E., Rumgay, H., Mafrá, A., Singh, D., Laversanne, M., Vignat, J., Gralow, J. R., Cardoso, F., Siesling, S., & Soerjomataram, I. (2022). *Current and future burden of breast cancer: Global statistics for 2020 and 2040*. *Breast (Edinburgh, Scotland)*, 66, 15–23.
- Attiq, N., Arshad, U., Brogi, S., Shafiq, N., Imtiaz, F., Parveen, S., Rashid, M., & Noor, N. (2022). *Exploring the anti-SARS-CoV-2 main protease potential of FDA approved marine drugs using integrated machine learning templates as predictive tools*. *International Journal of Biological Macromolecules*, 220, 1415–1428.
- Chun, K.-H., Park, J. H., & Fan, S. (2017). *Predicting and overcoming chemotherapeutic resistance in breast cancer*. *Translational Research in Breast Cancer*, 1026, 59–104.
- Daina, A., Michielin, O., & Zoete, V. (2017). *SwissADME: a free web tool to evaluate pharmacokinetics, drug-likeness and medicinal chemistry friendliness of small molecules*. *Scientific Reports*, 7, 42717.
- Deppeier, B., et al. (2002). *SPARTAN 02*. Wavefunction Inc.
- Faizi, M. S. H., Alam, M. J., Haque, A., Ahmad, S., Shahid, M., & Ahmad, M. (2018). *Experimental and theoretical characterization of organic salt: 2-((4-bromophenyl) amino) pyrido [1, 2-a] quinoxalin-11-ium bromide monohydrate synthesized via oxidative cyclization*. *Journal of Molecular Structure*, 1156, 457–464. <https://doi.org/10.1016/j.molstruc.2017.12.014>
- Floresta, G., Amata, E., Dichiarà, M., Marrazzo, A., Salerno, L., Romeo, G., Prezzavento, O., Pittalà, V., & Rescifina, A. (2018). *Identification of Potentially Potent Heme Oxygenase 1 Inhibitors through 3D-QSAR*

- Coupled to Scaffold-Hopping Analysis. *ChemMedChem*, 13(13), 1336–1342.
- Floresta, G., Cilibrizzi, A., Abbate, V., Spampinato, A., Zagni, C., & Rescificina, A. (2019). 3D-QSAR assisted identification of FABP4 inhibitors: An effective scaffold hopping analysis/QSAR evaluation. *Bioorganic Chemistry*, 84, 276–284.
- Gribble, G. W. (1996). *Pyroles and their benzo derivatives: applications*.
- Haque, A., Al-Balushi, R. A., Al-Busaidi, I. J., Khan, M. S., & Raithby, P. R. (2018). Rise of conjugated poly-ynes and poly (metalla-ynes): from design through synthesis to structure–property relationships and applications. *Chemical Reviews*, 118(18), 8474–8597. <https://doi.org/10.1021/acs.chemrev.8b00022>
- Haque, A., Rahman, M. A., Faizi, M. S. H., & Khan, M. S. (2018). Next Generation Antineoplastic Agents: A Review on Structurally Modified Vinblastine (VBL) Analogues. *Current Medicinal Chemistry*, 25(14), 1650–1662.
- Haque, A., Xu, L., Al-Balushi, R. A., Al-Suti, M. K., Ilmi, R., Guo, Z., Khan, M. S., Wong, W.-Y., & Raithby, P. R. (2019). Cyclometallated tridentate platinum (II) arylacetylides complexes: old wine in new bottles. *Chemical Society Reviews*, 48(23), 5547–5563.
- Jackson, S. M., Manolaridis, I., Kowal, J., Zechner, M., Taylor, N. M. I., Bause, M., Bauer, S., Bartholomaeus, R., Bernhardt, G., Koenig, B., Buschauer, A., Stahlberg, H., Altmann, K.-H., & Locher, K. P. (2018). Structural basis of small-molecule inhibition of human multidrug transporter ABCG2. *Nature Structural & Molecular Biology*, 25(4), 333–340. <https://doi.org/10.1038/s41594-018-0049-1>
- Laskowski, R. A., MacArthur, M. W., Moss, D. S., & Thornton, J. M. (1993). PROCHECK: a program to check the stereochemical quality of protein structures. *Journal of Applied Crystallography*, 26(2), 283–291. <https://doi.org/10.1107/S0021889892009944>
- Lee, S., et al. (2003). The PreADME Approach: Web-based program for rapid prediction of physico-chemical, drug absorption and drug-like properties. *EuroQSAR Designing Drugs and Crop Protectants: processes, Problems and Solutions*, 2003, 418–420.
- Lipinski, C. A. (2016). Rule of five in 2015 and beyond: Target and ligand structural limitations, ligand chemistry structure and drug discovery project decisions. *Advanced Drug Delivery Reviews*, 101, 34–41.
- Liu, W., Liu, X., Liu, W., Gao, Y., Wu, L., Huang, Y., Chen, H., Li, D., Zhou, L., Wang, N., Xu, Z., Jiang, X., & Zhao, Q. (2022). Discovery of novel β -carboline derivatives as selective AChE inhibitors with GSK-3 β inhibitory property for the treatment of Alzheimer's disease. *European Journal of Medicinal Chemistry*, 229, 114095.
- Mohammad, I. S., He, W., & Yin, L. (2018). Understanding of human ATP binding cassette superfamily and novel multidrug resistance modulators to overcome MDR. *Biomedicine & Pharmacotherapy=Biomedecine & Pharmacotherapie*, 100, 335–348. <https://doi.org/10.1016/j.biopha.2018.02.038>
- Moinul, M., Amin, S. A., Jha, T., & Gayen, S. (2022). Updated chemical scaffolds of ABCG2 inhibitors and their structure-inhibition relationships for future development. *European Journal of Medicinal Chemistry*, 241, 114628. <https://doi.org/10.1016/j.ejmech.2022.114628>
- Mushtaque, M., AVECILLA, F., Haque, A., Perwez, A., Khan, M. S., & Rizvi, M. M. A. (2017). Experimental and theoretical studies of a pyrazole-thiazolidin-2, 4-di-one hybrid. *Journal of Molecular Structure*, 1141, 417–427. <https://doi.org/10.1016/j.molstruc.2017.03.100>
- Nakanishi, T., & Ross, D. D. (2012). Breast cancer resistance protein (BCRP/ABCG2): its role in multidrug resistance and regulation of its gene expression. *Chinese Journal of Cancer*, 31(2), 73–99.
- Orlando, B. J., & Liao, M. (2020). ABCG2 transports anticancer drugs via a closed-to-open switch. *Nature Communications*, 11(1), 1–11. <https://doi.org/10.1038/s41467-020-16155-2>
- Patel, H., Wu, Z.-X., Chen, Y., Bo, L., & Chen, Z.-S. (2021). Drug resistance: From bacteria to cancer. *Molecular Biomedicine*, 2(1), 1–19. <https://doi.org/10.1186/s43556-021-00041-4>
- Schrödinger, L. (2012). *QikProp, version 3.5*.
- Song, H., Liu, Y., Liu, Y., Wang, L., & Wang, Q. (2014). Synthesis and antiviral and fungicidal activity evaluation of β -carboline, dihydro- β -carboline, tetrahydro- β -carboline alkaloids, and their derivatives. *Journal of Agricultural and Food Chemistry*, 62(5), 1010–1018.
- Spindler, A., Stefan, K., & Wiese, M. (2016). Synthesis and investigation of tetrahydro- β -carboline derivatives as inhibitors of the breast cancer resistance protein (ABCG2). *Journal of Medicinal Chemistry*, 59(13), 6121–6135.
- Taylor, N. M. I., Manolaridis, I., Jackson, S. M., Kowal, J., Stahlberg, H., & Locher, K. P. (2017). Structure of the human multidrug transporter ABCG2. *Nature*, 546(7659), 504–509.
- Tian, W., Chen, C., Lei, X., Zhao, J., & Liang, J. (2018). CASTp 3.0: computed atlas of surface topography of proteins. *Nucleic Acids Research*, 46(W1), W363–W367.
- Wang, J., Gong, F., Liang, T., Xie, Z., Yang, Y., Cao, C., Gao, J., Lu, T., & Chen, X. (2021). A review of synthetic bioactive tetrahydro- β -carbolines: A medicinal chemistry perspective. *European Journal of Medicinal Chemistry*, 225, 113815.
- Xing, X., et al. (2022). Discovery of Novel Tetrahydro- β -carboline Containing Aminopeptidase N Inhibitors as Cancer Chemosensitizers. *Frontiers in Oncology*, 12, 894842.